The capture yield of the ^{232}Th(n,γ) reaction measured at n_TOF-CERN

G. Aerts, E. Berthoumieux, F. Gunsing, L. Perrot
CEA/Saclay, DSM/DAPNIA/SPhN, F-91191 Gif-sur-Yvette, France
and the n_TOF Collaboration

May 19, 2004

Abstract

This report describes the analysis of the measurement of the ^{232}Th(n,γ) reaction, performed at nTOF-CERN in 2002. The analysis procedure to obtain the capture yield is detailed and the resulting cross section in the unresolved resonance region up to 1 MeV is given. The obtained cross section is independent from a reference capture measurement because of the self-normalization by means of a saturated resonance at low neutron energy. To check the analysis procedure, we performed identical steps for a gold sample measured in the same conditions. This measurement is part of experiment TOF07 [1].

1. Measurement setup and conditions

The measurements were done at the CERN-nTOF installation [2, 3] with two C_6D_6-detectors [4] placed perpendicular to the neutron beam. The samples were placed in a remotely controlled sample changer [5]. The distance from the center of the beam was 2.9 cm and the detectors were shifted from the center of the sample by 9.2 cm in order to reduce the scattered photon background.

Two thorium samples obtained from IRMM-Geel have been measured together at CERN. These samples have already been used at FZK-Karlsruhe for measurements [6]. The thickness of sample is such that some low-energy resonances are saturated from which the absolute normalization can be obtained. In addition to these samples, we used a natural lead sample to estimate the scattered photon background and a gold sample to verify the analysis procedure. The purity of Th sample was 99.5% according to the specifications. In table 1 the characteristics of the used samples are given.

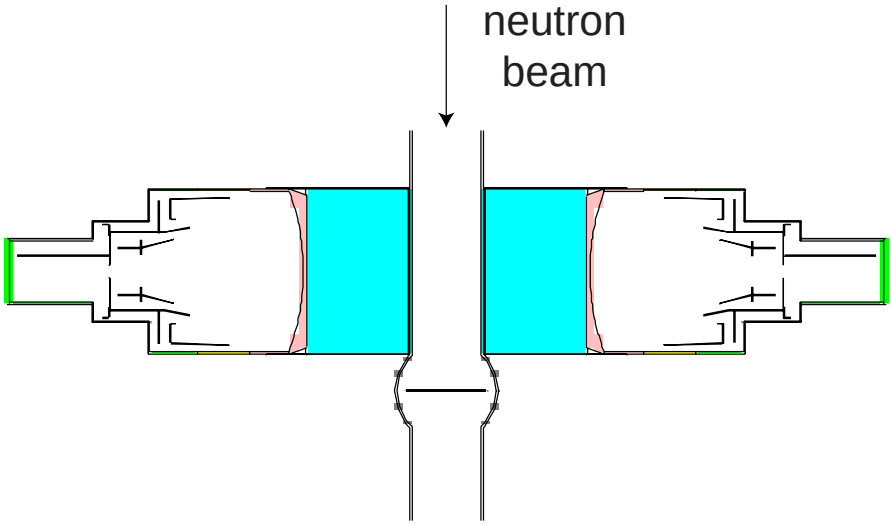

Figure 1: The geometry of the ^{232}Th(n,γ) measurement.

Table 1: Samples used in the experiments. For thorium and gold the two samples have been used together. The purity of 99.5% for Th is accounted for only in the total thickness expressed in at/b.

sample	diameter (cm)	mass (g)	calculated thickness (at/b)
^{232}Th	1.498	1.0262	$1.5112 \cdot 10^{-3}$
^{232}Th	1.498	1.7784	$2.6188 \cdot 10^{-3}$
^{232}Th total		2.8046	$\mathbf{4.1093 \cdot 10^{-3}}$
^{197}Au	1.504	0.8843	$1.5218 \cdot 10^{-3}$
^{197}Au	1.513	0.4454	$7.5791 \cdot 10^{-4}$
^{197}Au total		1.3297	$\mathbf{2.2798 \cdot 10^{-3}}$
^{nat}Pb	1.5485	2.0434	$3.1536 \cdot 10^{-3}$

2. Event selection and processing

The events from the runs listed in table 2 were processed from the DST files [7] and the amplitude and time-of-flight information for the C_6D_6 and silicon detectors was extracted. A pulse height weighting was applied to the C_6D_6 data to obtain a detector efficiency independent from the gamma-ray cascade following neutron capture.

3. Gamma-ray energy calibration

For the calibration of the pulse height distribution of the C_6D_6-detector we measured the response to radioactive sources of ^{137}Cs (0.662 MeV), ^{60}Co (1.173 and 1.332 MeV), and a composite source of ^{238}Pu together with carbon, giving a 6.13 MeV gamma-ray

Table 2: Run numbers used for the different samples.

sample	filter	run		
thorium (no beam)	-	3075	3171	
no sample (no beam)	-	3172		
Au	Al	3091	3092	
Th	Al	3098	3167	3168
Pb	-	3152		
Pb	Al	3153	3156	
Au	-	3090	3099	3101
		3106	3110	
		3138	3174	
Th	-	3093	3094	3095
		3096	3097	3100
		3102	3103	3109
		3115	3116	3117
		3118	3137	3140
		3149	3150	3160

through the ^{13}C(α, n)^{16}O* reaction.

With MCNP [8] we simulated the energy deposit in the scintillator volume to these gamma rays. The simulated spectra were broadened with a Gaussian function with a variance of the form $\sigma^2 = c_0 + c_1 E + c_2 E^2$ in order to take into account the effect of the photomultiplier. We obtained best results in fitting the function on the descending slope of the Compton edge. The adapted values, identical for both detectors, are $c_0 = 0, c_1 = 0.00374690\,\mathrm{MeV}^{-1}, c_2 = 0.00187140$.

The measured responses as a function of channel c were then matched to the simulated responses as a function of energy E_γ by fitting the channel to energy relation. Although the calibration is nearly linear, we found that the quadratic relation $E_\gamma = a_0 + a_1 c + a_2 c^2$ gave a better fit at low energies.

In figure 4 we show for both detectors the simulated broadened spectra together with part of the measured spectra after applying the channel to energy calibration.

Table 3: Energy calibration coefficients relating channel and energy by $E_\gamma = a_0 + a_1 c + a_2 c^2$.

	a_0	a_1	a_2
detector 1	0.0504370	0.0246315	$4.44452 \cdot 10^{-6}$
detector 2	0.0576934	0.027868	$4.93112 \cdot 10^{-6}$

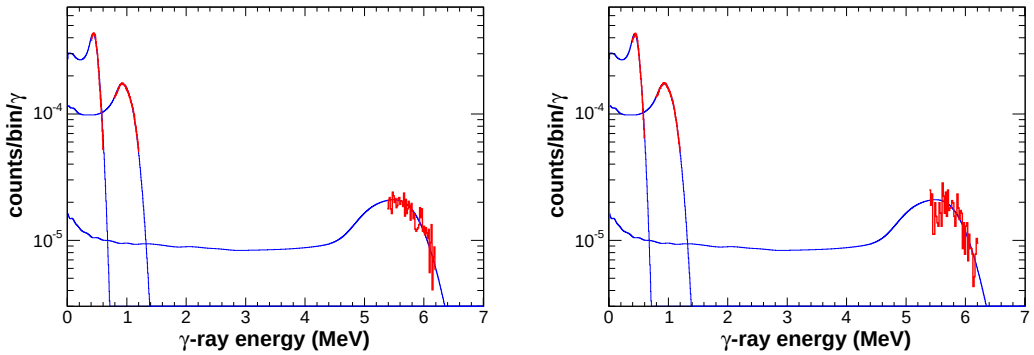

Figure 2: The simulated response functions (in blue) together with part of the measured spectrum (in red) for both detectors.

4. Weighting function calculation

The weighting function has been calculated [10] by Monte Carlo simulations of the detector response to mono-energetic gamma rays, using the code MCNP4C [8]. A fourth order polynomial was taken for the weighting function. The coefficients for the Th setup and the Au setup are listed in table 4. We have simulated the responses to 20 mono-energetic gamma rays up to 15 MeV in order to obtain a good fit also at higher energies from 7 to 10 MeV. The detector responses associated to these generated gamma rays have been convolved with the Gaussian broadening function described in the previous paragraph. The responses below a threshold of 160 keV, used in the event analysis, were not taken into account in the minimization procedure.

Table 4: Coefficients of the weighting function $W(E) = \sum a_i E_\gamma$ (with E_γ in MeV).

sample	a_0	a_1	a_2	a_3	a_4
Th	12.583	26.5247	33.141	-3.907	0.144
Au	8.907	34.3423	29.100	-3.415	0.140

5. Coincidence and dead time correction

The use of flash ADCs for the data acquisition should eliminate a possible dead time. Nevertheless, a small effective dead time in the order of a few tens of nanoseconds, related to the software pulse extraction, is still present. Its effect is often negligible, except at large local count rates, like in large resonances.

To estimate this effect, we calculated the distribution of the time between two consecutive events for each of the two detectors separately. The dead time can be estimated from this distribution, shown in figure 3. We also calculated the time distribution be-

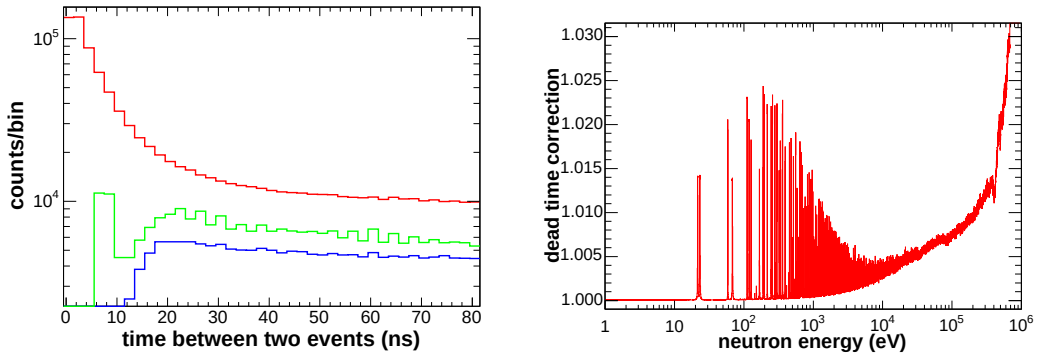

Figure 3: In the left panel the time distribution between two consecutive events for both detectors separately (blue and green) and for both detectors together (in red) is shown, revealing the coincidences and deadtime. In the right panel the resulting correction factor is shown for a fixed dead time of 30 ns and a threshold of 160 keV.

tween two consecutive events occurring in any of the two detectors. The distribution shows a pronounced peak below about 25 ns, revealing coincidences of two gamma rays of the same capture event. The coincidence events give rise to double counting of the capture event.

In the processing of the events, we discarded all events from both detectors within a fixed time $\tau = 30$ ns after the detection of an event. In this way we count only one of two coincident gamma rays and we have a sharply defined dead time for which can be corrected afterwards. The observed count rate spectrum $S_{\text{real}}(t)$ as a function of the time-of-flight t has to be corrected by a factor $f_\tau(t)$

$$f_\tau(t) = \frac{1}{1 - \frac{1}{N_b}\int_{t-\tau}^{t} S_{\text{observed}}(t')dt'} \tag{1}$$

where N_b is the number of bunches. The correction factor is shown in figure 1.

6. Relative normalization

The different spectra have to be normalized relative to each other in order to compare them. For this purpose a quantity is needed monitoring the number of neutrons incident on the target, or on a black resonance filter if any.

The number of incident neutrons is supposed to be proportional to the number of protons as well as the number of counts in the in-beam silicon flux monitor. The neutron flux measured by the SIMON detector [11] needs to be corrected for the loss of neutrons due to a black resonance filter. If the transmission of the filter is $T(E)$, the attenuation factor

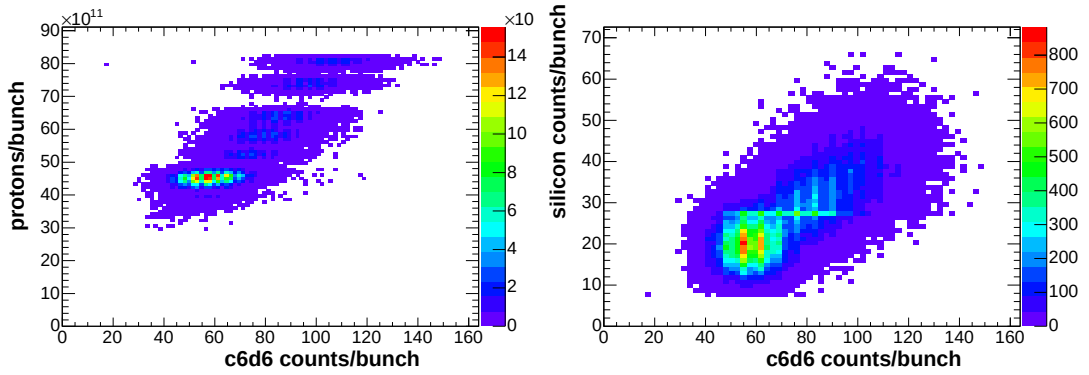

Figure 4: The counts per bunch as a function of one C_6D_6-detector and the number of protons (left panel) or number of counts in the silicon detector (right panel).

$f_n(E)$ is

$$f_n(E) = \frac{\int T(E)\Phi(E)Y_{(n,\alpha)}(E)\epsilon(E)dE}{\int \Phi(E)Y_{(n,\alpha)}(E)\epsilon(E)dE} \tag{2}$$

where $\Phi(E)$ is the neutron flux, $Y_{(n,\alpha)}(E)$ the reaction yield in the ^{6}Li-deposit and $\epsilon(E)$ the detection efficiency. We obtained $f_n = 0.7686$ integrating from 0.1 eV to 100 keV. This number is not very sensitive to small deviations on Φ, ϵ or Y since they cancel out in the ratio.

Comparing the two monitors for the same samples with and without the Al black resonance filter, we obtain a relative difference of 0.003 and 0.004 for the Th and Pb samples respectively and 0.06 for the Au sample. The latter is rather large but found to be related to erroneous proton information during the Au run, which we could confirm by checking the correlation of the protons and SIMON information with the count rate in the strong resonance at 4.9 eV. For the analysis we adopted the relative normalization obtained from the silicon detectors. Where needed, we applied a constant scaling factor to express the spectra in a standard way to $7 \cdot 10^{12}$ protons per bunch.

In figure 4 a histogram of the number of protons and one of the counts in the silicon detectors versus the counts in one of the C_6D_6 detectors for each pulse is shown. In this case with good statistics, the correlation is nearly equal and close to unity. For the shorter runs however, and especially during the gold runs because of a temporary problem of read-out of the proton information, the scatter is much less for the silicon monitors than for the protons.

In our analysis procedure the relative normalization is important only for the determination of the attenuation of the in-beam gamma rays by the Al filter in the beam, obtained by the Pb measurements with and without a filter in the beam. We have used the silicon

detector information for this normalization.

7. Background parametrization

Several components contribute to the background. The radioactivity of the sample has been measured with the neutron beam switched off. The gamma-ray spectrum of our ^{232}Th samples have gamma-ray energies going up to 2.6 MeV originating from the beta decay of the daughter product ^{208}Tl. This presents a constant background in time and is visible as a decreasing line when represented as a function of the equivalent neutron energy. With the high instantaneous flux of the n_TOF installation this background is relevant only at low neutron energies and can be easily subtracted or fitted with the data.

The main source of background in the keV region comes from in-beam gamma rays scattered from the sample and detected in the C_6D_6-detectors. Measurements have been taken of the thorium sample with and without neutron filters in the beam. The neutron filters remove the neutrons at specific energies, corresponding to large resonances of the filters with zero transmission, the so-called black resonances. We have used measurements with a 30 mm thick aluminum filter. The level of the background in the measurements with filters corresponds to the valleys of the black resonances. But the neutron filter also attenuates the in-beam photons that are scattered from the sample. In order to obtain the level of the background in the measurements without filters, we have to correct for the attenuation of the in-beam gamma-rays by the filters.

The general shape of the background as a function of the time of flight t was described by the sum of three components.

$$B(t) = a_1 t^{b_1} + a_2 \exp(b_2 \cdot t) + a_3 \exp(b_3 \cdot t) \tag{3}$$

The first term, from now on denoted as $B_l(E)$, is dominant at low equivalent neutron energies E while the two other terms, associated with a sample scattered photon background and denoted as $B_\gamma(E)$, become the most important background source in the keV region. The two contributions to the background $B(E)$ can be written as

$$B(E) = B_l(E) + B_\gamma(E) \tag{4}$$

In the following it is assumed that the shape of the sample scattered photon background $B_\gamma(E)$ is independent of the sample. Only the level depends on the sample. On the contrary the shape of the low-energy part $B_l(E)$ depends on the sample and is extracted from the resonance region below 100 eV. With these assumptions the background in the thorium spectrum, after correction for the radioactivity background, can be written as

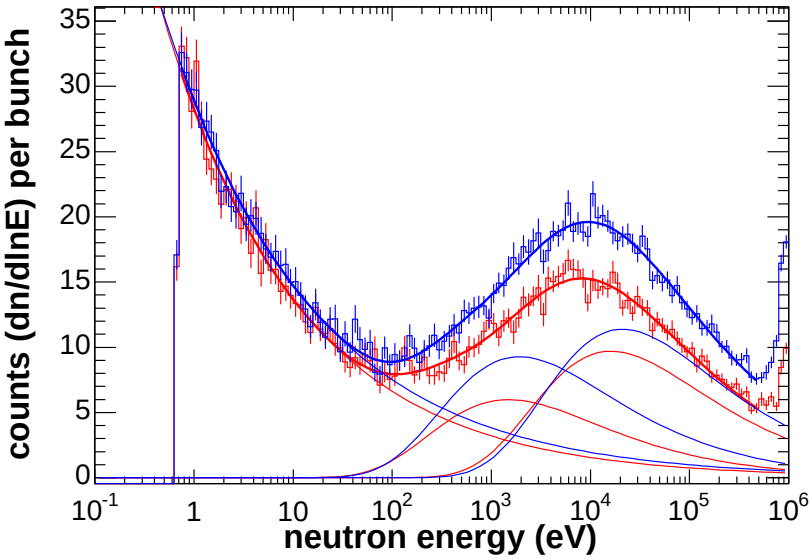

Figure 5: The fitted shape of the background together with the three separate components of each fit for the Pb sample (in blue) and for the Pb sample with Al filter (in red) with a threshold of 160 keV.

$$B_{\mathrm{Th}}(E) = B_{\mathrm{Th},l}(E) + B_{\mathrm{Th},\gamma}(E) = B_{\mathrm{Th},l}(E) + \frac{1}{f_\gamma(E)} \cdot B_{\mathrm{ThAl},\gamma}(E) = B_{\mathrm{Th},l}(E) + \frac{f_1}{f_\gamma(E)} \cdot B_{\mathrm{Pb},\gamma}(E) \quad (5)$$

where $f_\gamma(E)$ is the attenuation of the in-beam gamma rays due to the in-beam Al neutron filter, and where f_1 presents a scaling factor.

The shape of the background is given by a measurement under the same conditions using a sample of natural lead. Its capture cross section is rather low and the reaction rate in the keV region is almost entirely due to sample scattered in-beam photons. Measurements of a lead sample have been taken with and without the filters in the beam. After subtraction of the expected capture yield, which is small compared to the background, we could fit the scattered photon background in lead with and without filters $B_{\mathrm{Pb}}(E)$ and $B_{\mathrm{PbAl}}(E)$ according to eq. (3). We fitted this background function to the two spectra of lead samples with 1.5 cm diameter with and without the Al filter in the beam. The result of the fits is shown in figure 5.

The attenuation of the gamma-ray spectrum as a function of equivalent neutron energy $f_\gamma(E)$ can be then be found from the background in the lead spectra from the ratio

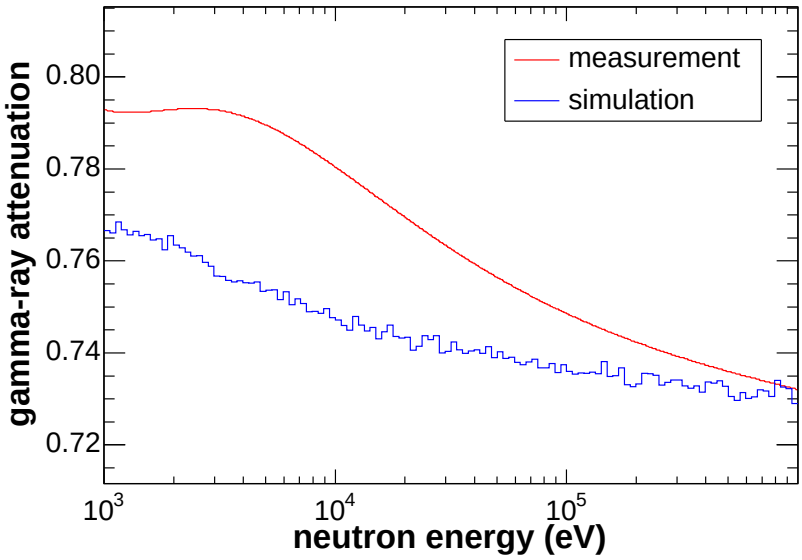

Figure 6: The attenuation due to the Al filter of the detected sample scattered photons background.

$$f_\gamma(E) = \frac{B_{\mathrm{PbAl},\gamma}(E)}{B_{\mathrm{Pb},\gamma}(E)} = \frac{B_{\mathrm{PbAl}}(E) - B_{\mathrm{PbAl},l}(E)}{B_{\mathrm{Pb}}(E) - B_{\mathrm{Pb},l}(E)} \tag{6}$$

We verified this procedure by simulating the energy deposit in the C_6D_6-detectors from a gamma-ray spectrum incident on the samples, with and without prior attenuation by the filters. We used the gamma-ray spectrum as a function of time-of-flight resulting from previous detailed simulations [12]. From the Monte Carlo simulations we found that there is no noticeable difference in the shape when using the Pb, Th or Au sample. The measured and simulated attenuation factor, shown in figure 6, agree within a few percent. In the analysis we have used the measured attenuation.

The factor f_1 presents the scaling, assumed to be constant, of the background of the lead sample $B_{\mathrm{Pb},\gamma}(E)$ to the level of thorium with Al filter and can be written as

$$f_1 = \frac{B_{\mathrm{ThAl},\gamma}(E)}{B_{\mathrm{Pb},\gamma}(E)} = \frac{B_{\mathrm{ThAl}}(E) - B_{\mathrm{ThAl},l}(E)}{B_{\mathrm{Pb}}(E) - B_{\mathrm{Pb},l}(E)} \tag{7}$$

This expression contains the background of the thorium sample and of the lead sample. While for lead this background can be easily estimated after subtraction of the expected capture yield, for thorium we have used the black resonance filters. At the black resonance of Al at 34.8 keV all neutrons are removed from the beam and what the remaining part is the background. With the Pb sample this is not visible, since nearly all the signal is background, but with the Th sample a clear dip is visible in the spectrum. We

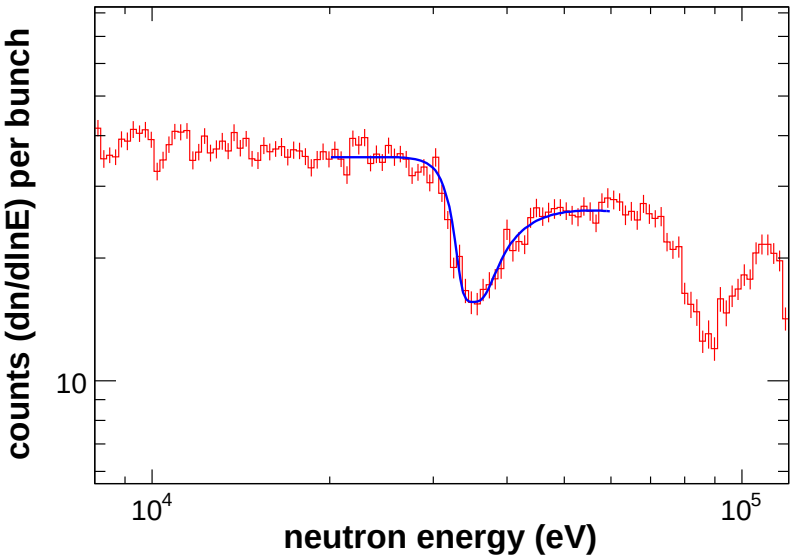

Figure 7: Part of the spectrum of the Th sample with the Al filter in the beam and the fit of the 34.8 keV black resonance of Al.

calculated f_1 from eq. (7) evaluated at $E = 34.8$ keV.

We determined the level of the dip due to the black resonance in the thorium with filter spectrum by fitting the expected shape of the resonance as a perturbation on a smooth reaction yield. The expected shape was calculated as a transmission using the total cross section of Al without the potential scattering contribution. In figure 7 the spectrum of the Th sample with the Al filter in the beam in the vicinity of the 34.8 keV resonance of Al is shown together with the fit from which we determine the level. The uncertainty for this level, obtained from the fit and the variation from different binnings, is about 2.5%.

The component at low energies $B_l(E)$ has been determined by subtracting the expected capture yield in the off-resonance region in the vicinity of the first resonance of thorium. Although this requires the use of the capture cross section which we want to measure, a rough estimate is sufficient since this component contributes to less than 10% to the background in the keV region.

Finally we compared this background estimation with the more simple procedure of applying the scaling factors directly to the background $B(E)$ without a separation into two components. In the keV region this simplified procedure corresponds to within a few %.

The resulting background is shown in figure 8 together with the uncorrected capture rate in the unresolved resonance region.

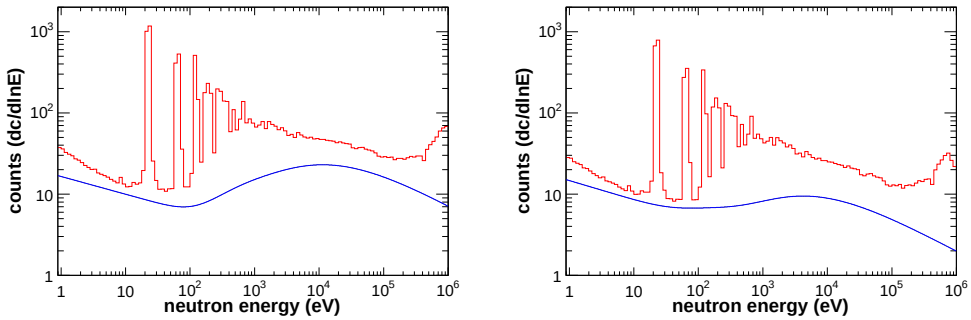

Figure 8: The signal and background for the thorium data with a threshold of 160 keV (left) and 1000 keV (right).

8. Flux determination

In order to determine the capture yield, the shape of the neutron flux is needed. Since the absolute normalization in our analysis is obtained from a low-energy saturated resonance, the absolute value of the flux is not necessary but only the relative energy dependence. On the contrary we need the shape of the flux from approximately 1 eV up to 1 MeV.

Several measurements of the neutron flux have been performed in addition to Monte Carlo simulations [12]. At present, the data of two in-beam flux measurements covering a large energy range are available. One is a measurement from 2001 with a parallel plate ionization chamber from the Physikalisch-Technische Bundesanstalt Institut (PTB) using the fission reaction on ^{235}U. The other is the measurement of the flux by the SIMON detectors consisting of a 200 μg/cm^2 ^{6}Li deposit on a mylar foil put in the beam. The reaction products of the ^{6}Li(n,^{3}H)α reaction, considered a standard up to 100 keV, are detected by 4 off-beam silicon detectors [11]. Data from the PPACs fission detector with the collimation of the capture experiments have not been exploited yet.

The data from the PTB measurement are available as a point-wise neutron flux[12]. The data from the silicon monitors have been processed to extract the triton events [14]. An energy dependent efficiency was then applied taking into account also the angular distribution of the α and triton particles [13]. The reaction rate was converted to the neutron flux using the cross section standard.

In a first attempt both measurements have been fitted with a smooth analytical function, multiplied by the transmission through the aluminum window in the beam near the neutron source calculated on an energy grid of 5000 points per decade. The fit is more or less satisfactory up to about 200 keV. At higher energies, the structures in the flux, partly due to neutron absorption by oxygen from the water moderator, are not well described.

By comparing the two fits of the neutron flux, with the fit of the SIMON flux normalized

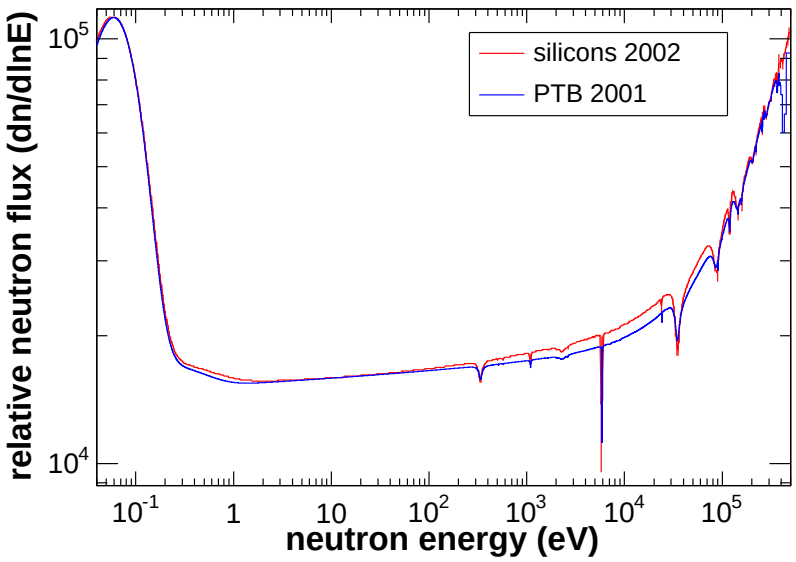

Figure 9: Comparison of the fitted flux measured by PTB in 2001 and by the SI-MON detectors in 2002.

to the fit of the PTB flux at 4.9 eV, we observe a slightly different energy dependence for both data sets, shown in figure 9. Although the thermal peak below 0.1 eV coincides, the difference in energy dependence is clearly visible in the region around 10 keV where it is about 7%. This difference can be explained by the angular distribution corrections to be applied to the silicon data. Although the reaction products are isotropic up to about 1 keV, above this energy the angular distribution is not well known.

On the other hand, the PTB data show at lower energies more scatter than the silicon data, probably due to lack of statistics and the complex resonance structure. In addition, the dip around 300 eV due to the manganese impurity in the aluminum alloy window in the beam is visible only in the silicon data but not in the PTB data as shown in the the left panel of figure 10.

In the right panel of this figure we show again the original data points from the the PTB and the silicon measurements and we have added the flux extracted from the gold data taken in this setup, using the cross section in the 10-100 keV region.

Finally we decided to use the flux fitted from the silicon data up to 1 keV and use the point-wise PTB flux at higher energies.

9. Capture yield

From the experimental spectra we obtain the capture yield of the thorium measurement by

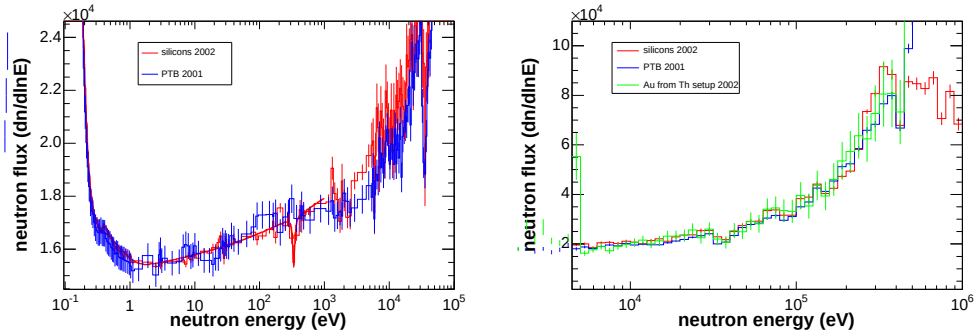

Figure 10: Comparison of the measured flux by PTB in 2001 and by the SIMON detectors in 2002.

$$Y(E) = N \times \frac{S_{\mathrm{Th}}(E) - B_{\mathrm{Th}}(E)}{C(E) \times f_b(E) \times \Phi(E)} \tag{8}$$

where S_{Th} is the thorium spectrum, B_{Th} its background, $\Phi(E)$ the neutron flux, and N the absolute normalization obtained from a low-energy saturated resonance. The factor $C(E)$ contains the corrections due to self absorption and multiple scattering effects in the unresolved resonance region and $f_b(E)$ the fraction of incident flux corresponding to the change of the neutron beam profile with energy.

The capture yield as a function of the neutron energy E is related to the cross sections by

$$Y(E) = \mu(E)\left(1 - e^{-n\sigma_T(E)}\right) \cdot \frac{\sigma_\gamma(E)}{\sigma_T(E)} \tag{9}$$

where σ_γ is the capture and σ_T the total neutron cross section, and where $\mu(E)$ is the energy dependent multiple scattering correction. In the resolved resonance region the cross section is described by resonance parameters fitted with a code like SAMMY [18] from the capture yield, taking into account the experimental effects.

In the unresolved resonance region the cross section, obtained from the yield after corrections, is usually reported as point-wise data to which a smooth curve from a Hauser-Feshbach calculation can be fitted with a code like FITACS [20] with a limited number of average parameters like the level density, the average radiation width and the neutron strength functions.

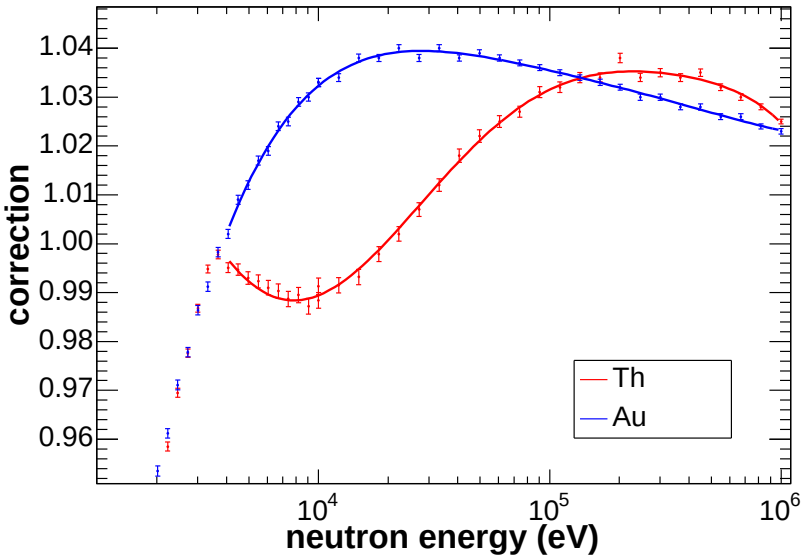

Figure 11: The correction on the capture cross section due to self absorption and multiple scattering calculated from SESH [19].

10. Self absorption corrections

The average capture yield $< Y(E) >$ in the unresolved resonance region can be expressed as

$$< Y(E) >= n \times \sigma_\gamma(E) \times C(E) \tag{10}$$

where $C(E)$ is a correction that needs to be applied to account for self absorption and multiple scattering effects. We used the code SESH [19] to calculate the correction to apply to $\sigma_\gamma(E)$ as obtained from equation 10. Unlike a code like MCNP [8], SESH generates individual resonances, important to estimate this effect, in the unresolved resonance region and does not use smooth cross sections. For this reason we have adopted the corrections calculated from SESH, shown in figure 11 together with an empirical fit we applied to the data.

11. Beam fraction correction

The fraction of the neutron beam incident on the sample has an energy dependence due to the change of the beam profile [15]. We calculated the beam profile from the original simulations [12] for several energy regions [16]. From these profiles we calculated the fraction of neutron incident on a circle with diameter 1.5 cm. This fraction was then fitted to obtain a smooth function as shown in figure 12.

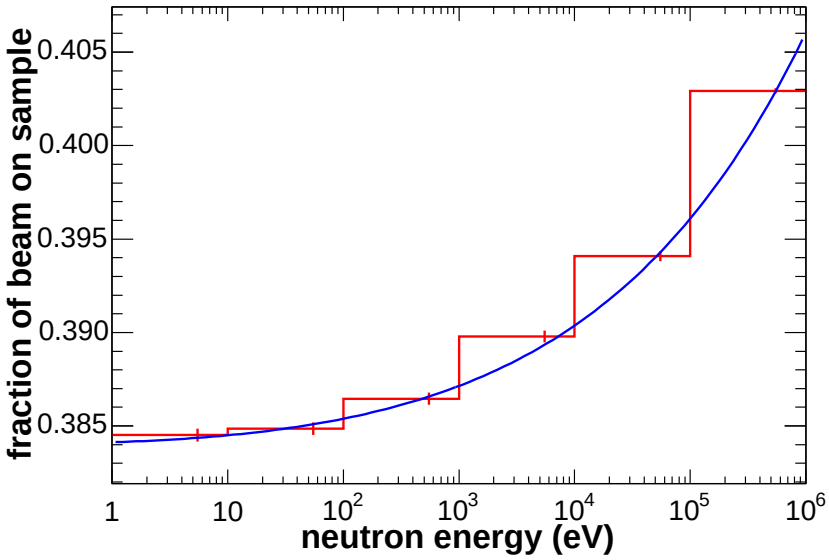

Figure 12: The fraction of neutrons incident on a sample with diameter 1.5 cm.

12. Absolute normalization

We extracted the absolute normalization from low-energy saturated resonances. When fitting the resonance, the normalization is not a scaling factor of the capture kernel but can be fitted with less correlation to the resonance parameters. We used the code SAMMY for the resonance analysis [18]. For gold, for which the 4.9 eV resonance is often used because of its saturated resonance, the resonance parameters from the libraries are known not to be exact [17]. In fitting the normalization from this resonance, we let free also the neutron width Γ_n, which substantially increased the quality of the fit.

In the same way we fitted the normalization of thorium on two saturated resonance around 20 eV. The results of the fit are shown in figure 13. The normalizations in gold and thorium were fitted with a 0.3% statistical uncertainty. For both samples the normalizations were different by about 1.1% which can be attributed to the threshold corresponding to a different fraction of the gamma-ray spectrum.

13. The cross section in the unresolved resonance region

Performing all the steps and corrections described before, we obtain the cross section in the unresolved resonance region independently for both thorium and, with much less statistics, gold. In figures 15 and 14 these cross sections are given for both isotopes.

Although the spectra are shown up to 1 MeV it should be noted that the cross section contains also contributions from inelastic scattering. For the thorium measurement the

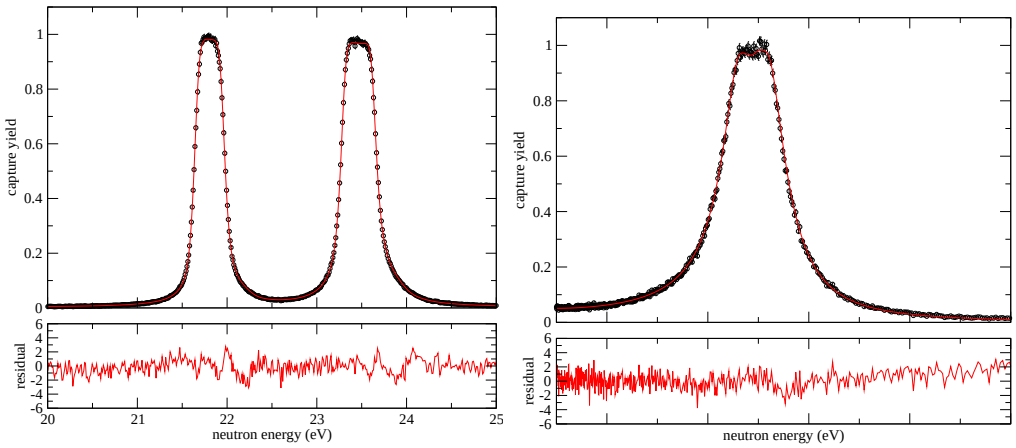

Figure 13: The normalization fitted from saturated resonances in thorium (left panel) and gold (right panel).

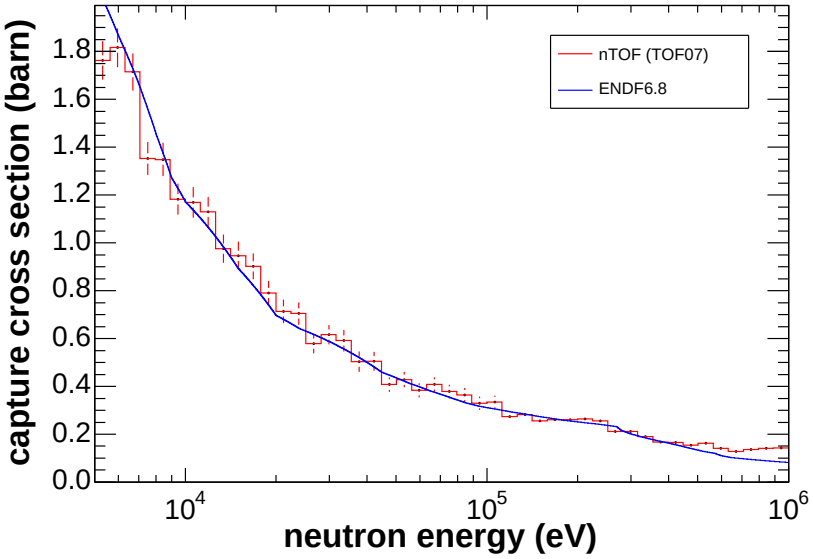

Figure 14: The measured cross section for gold (threshold 160 keV) compared with some of the other measurements and evaluations.

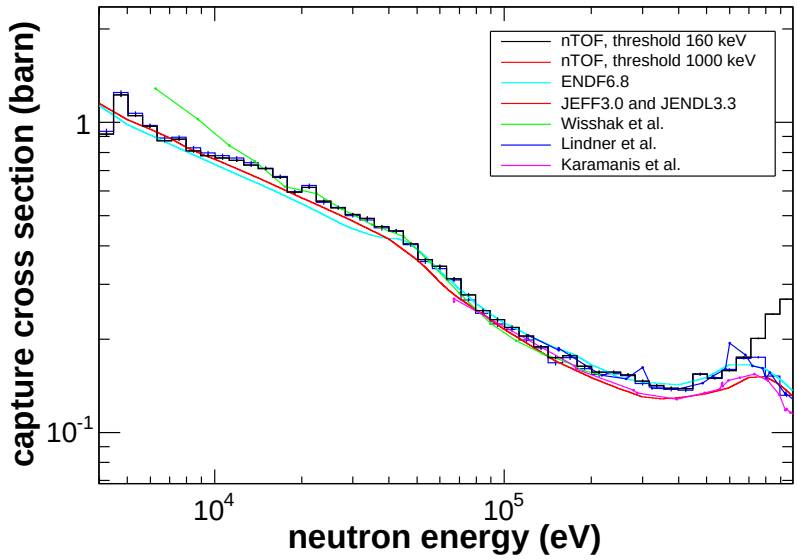

Figure 15: The measured cross section for thorium (thresholds 160 keV and 1000 keV) compared with some of the other measurements and evaluations.

first level is at 49 keV but is excluded by the threshold of 160 keV. The next levels have a lower (n, n′, γ) cross section because of spin parity considerations. Above about 600 keV the gamma rays from inelastic scattering become visible in our spectrum. Repeating the analysis with a threshold of 1 MeV removes the contributions of the from inelastic scattering below 1 MeV, but at the expense of a reduction of the statistics. Below about 600 keV however, the resulting cross sections remain the same within the error bars. As a final cross section we used the data with a gamma-ray threshold of 160 keV up to 300 keV neutron energy, and a threshold of 1 MeV at higher energies.

Then we used the code FITACS [20] to fit the cross section with average resonance parameters. Keeping the average radiation width and level density fixed with the evaluated values, we fitted only the neutron strength functions S_0, S_1 and S_2. The result of the fit is shown in figure 16. More up-to-date values of the average radiation width and level density, including a missing level estimation, will follow from the resonance analysis.

14. Uncertainties

The total uncertainty on the cross section consists of several contributions that can be identified from the analysis procedure. The main sources come from the background determination and from the applied flux.

The uncertainty related to the influence of the weighting function is rather small in this case since the measurement is not relative to a different isotope, in which case

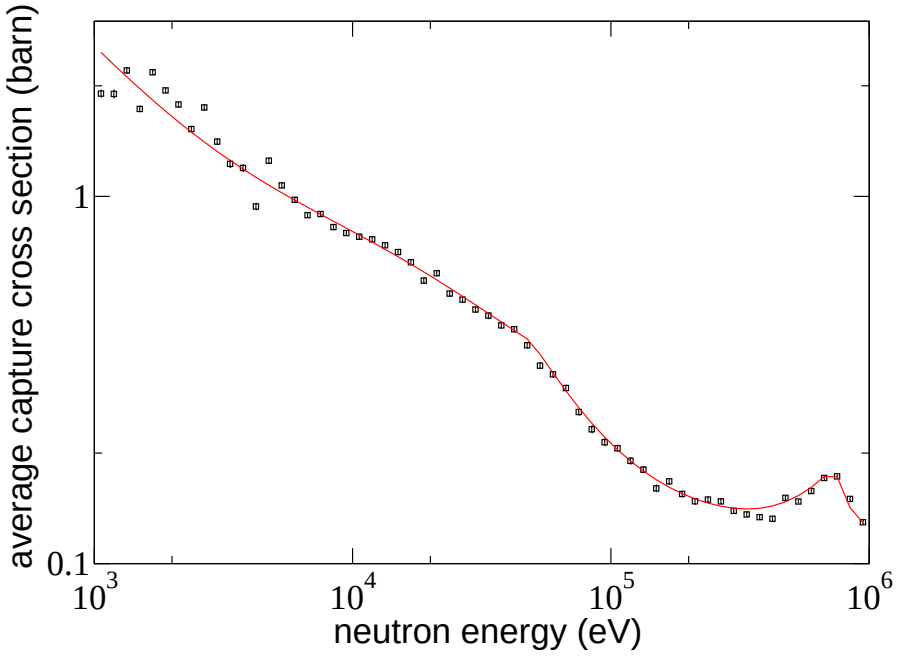

Figure 16: The ^{232}Th(n,γ) cross section in the unresolved resonance region, obtained with a gamma-ray threshold of 1 MeV, together with a fit of the neutron strength functions $S_{\ell=0,1,2}$.

commonly about 3% is attributed. The gamma-ray spectra are quite similar as a function of neutron energy, due to the large number of levels available for decay after capture, The influence of the threshold may play a role, but the resulting cross section with a low or high threshold give statistically coherent results. We assign an uncertainty of 0.5% to the weighting function.

The uncertainty due to background subtraction is the most delicate to estimate. The absolute level of the background requires the determination of the level of the black resonance. The sample scattered photon background estimation requires the subtraction of the expected capture yield of lead. We applied several combinations of fits and binnings of the spectrum and we estimate the uncertainty on the background subtraction to 3%. This value is also in agreement with the maximum difference in cross section obtained with a threshold of 160 keV and 1000 keV.

It is more difficult to obtain a good estimate on the precision of the flux determination. For the moment we adopt an uncertainty of 4% to the used neutron flux.

References

[1] *Measurement of the neutron capture cross section of ^{232}Th, ^{231}Pa, ^{234}U and ^{236}U*, U. Abbondanno et al. Technical Report CERN/INTC 2002-010, CERN, 2002.

Table 5: Estimated systematic uncertainties on the ^{232}Th(n,γ) cross section.

source	estimated (%)
weighting function	0.5
background subtraction	3
flux	4
total	5

proposal.

[2] *Results from the commissioning of the n_TOF spallation neutron source at CERN*, C. Borcea *et al. , Nucl. Instr. Meth. A* **513** (2003) 524-537

[3] U. Abbondanno et al. CERN n_TOF facility: Performance report. Technical Report CERN/INTC-O-011; INTC-2002-037; CERN-SL-2002-053 ECT, CERN, 2003.

[4] *An optimized C_6D_6 detector for studies of resonance-dominated (n,γ) cross-section*, R. Plag, M. Heil, F. Käppeler, P. Pavlopoulos, R. Reifarth, and K. Wisshak, and The n_TOF Collaboration, *Nucl. Instr. Meth. A* **496** (2003) 425-436

[5] *Results from the commissioning of the n_TOF spallation neutron source at CERN*, P. Milazzo *et al. , Nucl. Instr. Meth. B* **213** (2004) 36-41

[6] K. Wisshak, F. Voss, and F. Käppeler, *Nucl. Sci. and Eng.* **137** (2001) 183

[7] *Pulse Shape Analysis Routine Prototype for Carbon Fiber C6D6 detectors*, D. Cano-Ott, DST version 5

[8] J. F. Briesmeister, Ed., *MCNP - A General Monte Carlo N-Particle Transport Code, Version 4C3*, LA-13709-M (2000)

[9] *New experimental validation of the pulse height weighting technique for capture cross-section measurements*, U. Abbondanno *et al. , Nucl. Instr. Meth. A* **521** (2004) 454-467

[10] *Weighting functions for the neutron capture measurements performed at n TOF-CERN in 2002-2003*, G. Aerts, *et al.* , internal report DAPNIA-04-106, 2004

[11] *A low background neutron flux monitor for the n_TOF facility at CERN*, S. Marrone *et al. , Nucl. Instr. Meth. A* **517** (2004) 389-398

[12] V. Vlachoudis, private communication

[13] N. Colonna, private communication

[14] *Neutron fluence distribution from the SiMon in TOF07*, n_TOF analysis group report, L. Perrot *et al.* , 2002

[15] Measurement of the n_TOF beam profile with a micromegas detector, J. Pancin et. al, *Nucl. Instr. Meth. A* **524** (2004) 102-114

[16] J. Pancin, private communication

[17] M. C. Moxon, private communication

[18] N. M. L. Larson, *SAMMY: Multilevel R-Matrix Fits To Neutron Data Using Bayes Equation*, ORNL/TM-9179/R5, (2001).

[19] F. H. Fröhner, SESH, computer code, Report GA-8380, 1968

[20] F. H. Fröhner, B. Goel and U. Fischer, FITACS, computer code, Report ANL-83-4, 1983

[21] F. Rahn *et al.* , *Phys. Rev. C* **6** (1972) 1854

[22] M. Lindner *et al.* , *Nucl. Sci. and Eng.* **59** (1976) 381

[23] R. L. Macklin and J. Halperin,, *Nucl. Sci. and Eng.* **64** (1977) 849

[24] P. Poenitz, ANL/NDM-45 (1978)

[25] K. Kobayashi *et al.* , *J. Nucl. Sci. Techn.* **18** (1981) 823

[26] R. L. Macklin, *Nucl. Sci. Eng.***79** (1981) 118

[27] D. K. Olsen, R. W. Ingle, J. L. Portney, *Nucl. Sci. Eng.* **82** (1982) 289

[28] R. B. Perez *et al.* , *Nucl. Sci. and Eng.* **80** (1982) 189

[29] K. Kobayashi *et al.* , *Ann. Nucl. Energy* **15**(8) (1988) 381

[30] Yu. V. Grigoriev *et al.* , *Proc. Int. Sem. Interact. Neutrons with Nuclei, ISINN-8* , Dubna (2000) 68

[31] D. Karamanis *et al.* , *Nucl. Sci. and Eng.* **139** (2001) 282

[32] V. Maslov, http://www-nds.iaea.or.at/minskact/